

# Thermal Management in Plug-In Hybrid Electric Vehicles: a Real-Time Nonlinear Model Predictive Control Implementation

J. Lopez-Sanz, Carlos Ocampo-Martinez *Senior Member, IEEE*, Jesus Alvarez-Florez, Manuel Moreno-Eguilaz, Rafael Ruiz-Mansilla, Julian Kalmus, Manuel Gräber, Gerhard Lux

**Abstract**—A real-time nonlinear model predictive control (NMPC) for the thermal management (TM) of the electrical components cooling circuit in a Plug-In Hybrid Electric Vehicle (PHEV) is presented. The electrical components are highly temperature-sensitive and therefore working out of the ranges recommended by the manufacturer can lead to their premature aging or even failure. Consequently, the goals for an accurate and efficient TM are two: to keep the main component, the Li-ion battery, within optimal working temperatures, and to consume the minimum possible electrical energy through the cooling circuit actuators. This multi-objective requirement is formulated as a finite-horizon optimal control problem (OCP) that includes a multi-objective cost function, several constraints and a prediction model especially suitable for optimization. The associated NMPC is performed on real-time by the optimization package MUSCOD-II and is validated in three different repeatable test-drives driven with a PHEV. Starting from identical conditions, each cycle is driven once being the cooling

circuit controlled with NMPC and once with a conventional approach based on a finite-state machine. Compared to the conventional strategy, the NMPC proposed here results in a more accurate and healthier temperature performance, and at the same time, leads to reductions in the electrical consumption up to 8%.

**Index Terms**—nonlinear model predictive control (NMPC), thermal management, plug-in hybrid electric vehicles (PHEV), Li-ion battery cooling.

## I. INTRODUCTION

IN electrified vehicles, an accurate TM of the electric traction components is crucial to avoid premature costly repairs and ensure safety and performance requirements [1]. Among them, the Li-ion battery package is the most critical due to its cost and its direct relation to the vehicle autonomy, which is definitely the electromobility market penetration bottleneck. Accurate TM solutions for Li-ion batteries are based usually on liquid cooling systems with complex pipes configurations that allow several options for heat dissipation. To control these circuits, multiple electrical actuators are needed. Since a misuse of electrical actuators contributes to a further decrease in vehicle autonomy, optimal control methods become quite attractive for accurate and efficient TM. Compared to the classical approach of using tuned Proportional-Integral-Derivative (PID) controllers according to a set of rules learned from experience, optimization-based methods such as NMPC exploit their potential in systems with:

- multiple inputs multiple outputs (MIMO).
- several goals that can be contradictory.
- numerous constraints that must be fulfilled, among others.

Although the many advantages, there are also some challenges for NMPC to spread in the automotive sector. The computational burden is one of them. A proof of this fact is the large number of existing offline applications in literature compared to the online category. Moreover, it

J. Lopez-Sanz and G. Lux are with Innovation and Alternative Mobility Department, SEAT Technical Center, Autovia A-2, Km. 585 Apdo. de Correos 91, 08760 Martorell, Spain, e-mails: [extern.jorge.lopez@seat.es](mailto:extern.jorge.lopez@seat.es), [gerhard.lux@seat.es](mailto:gerhard.lux@seat.es)

C. Ocampo-Martinez is with Automatic Control Department, Universitat Politècnica de Catalunya, Institut de Robòtica i Informàtica Industrial (CSIC-UPC), Llorens i Artigas, 4-6, 08028 Barcelona, Spain, e-mail: [cocampo@iri.upc.edu](mailto:cocampo@iri.upc.edu)

J. Alvarez-Florez is with the Center for Engines and Heat Installation Research (CREMIT), Technical University of Catalonia, Barcelona Tech., 08028 Barcelona, Spain, e-mail: [jalvarez@mmt.upc.edu](mailto:jalvarez@mmt.upc.edu)

M. Moreno-Eguilaz is with the Center Innovation Electronics, Motion Control and Industrial Applications (MCIA), Technical University of Catalonia, Barcelona Tech., 08028 Barcelona, Spain, e-mail: [manuel.moreno.eguilaz@upc.edu](mailto:manuel.moreno.eguilaz@upc.edu)

R. Ruiz-Mansilla is with the Green Technologies Research Group (GREENTECH), Technical University of Catalonia, Barcelona Tech., 08028 Barcelona, Spain, e-mail: [rafael.ruiz@upc.edu](mailto:rafael.ruiz@upc.edu)

J. Kalmus works at TLK-Thermo GmbH, Hans-Sommer-Str.5, 38106 Braunschweig, Germany, e-mail: [j.kalmus@tlk-thermo.de](mailto:j.kalmus@tlk-thermo.de)

M. Gräber works at TLK Energy GmbH, Steppenbergrweg 30, 52074 Aachen, Germany, e-mail: [manuel.graerber@tlk-energy.de](mailto:manuel.graerber@tlk-energy.de)

This work was supported by the catalan Government: la Generalitat de Catalunya. Corresponding author: Jorge Lopez-Sanz [extern.jorge.lopez@seat.es](mailto:extern.jorge.lopez@seat.es)

Manuscript received XXX; revised XXX.

is common that real-time capable NMPC applications are not validated directly in the real vehicle, but in a simpler context. This is the case of [2], where NMPC for adaptive cruise control is tested in a Hardware in the Loop (HIL) configuration on a dynamic engine test bench or [3], where an NMPC application for optimal trajectory generation in Long Heavy Vehicles Combinations that validated the controller in a motion simulator. In [4], the real-time NMPC strategy for an hybrid electric vehicle (HEV) power management is validated in simulations and the same is done in [5] to show the potential of NMPC for HEV fuel and emissions minimization. The validation through simulation/test bench environments in all these examples and many more is a necessary first step for every real-time application.

The purpose of this article is to use NMPC for the TM of the Li-ion battery (BAT) and the power electronics (PE) in a PHEV prototype. The validation of the feedback control designed by using the optimization tool MUSCOD-II [6] is done by means of a comparison to a finite-state machine control. The novelty of this paper is that the optimizer runs on an Intel®Core™ i5-3320M Processor with the two cores operating at 2.6 GHz and with 8 GB of RAM on real-time and overtakes the TM control by means of an electronic control unit (ECU) bypass performed on a rapid prototyping (RP) module. This NMPC implementation corresponds to a new step in the NMPC standardization road map suggested in Fig. 1, where the final goal is to have the algorithm running embedded in the vehicle. In this sense, [7] points FPGA or multicore microprocessors as the suitable platforms to exploit parallelization of the NMPC controller design.

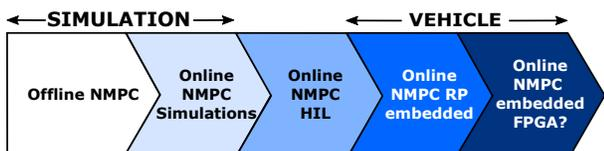


Fig. 1: NMPC roadmap in the automotive sector.

The remainder of this paper is structured as follows. Section II presents a brief description of the control plant. Section III gives an overview of the model, more extensively treated in [8], and defines the goals and constraints of the control problem. Section IV deals with the numerical solution of the NMPC problem. In Section V, the hardware implementation in the vehicle is presented and Section VI describes the driving scenarios in which validation took place. Finally, Section VII shows the results and the conclusions and final remarks are drawn in Section VIII.

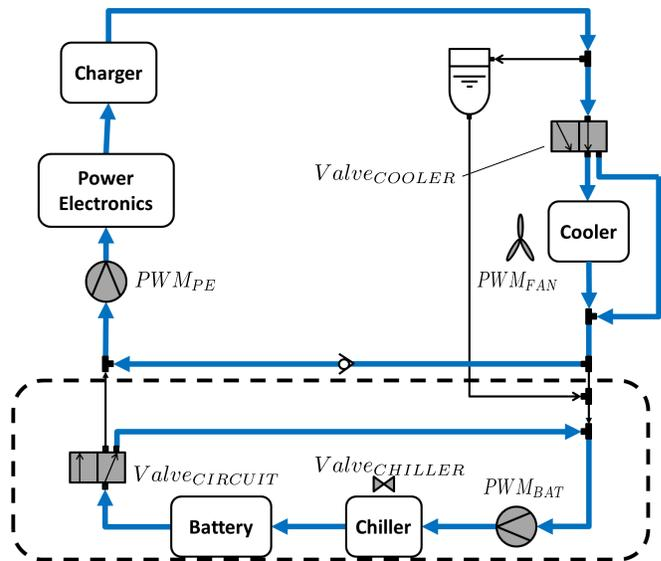


Fig. 2: The studied cooling circuit.

## II. PROBLEM STATEMENT

The cooling circuit to be controlled by NMPC can be seen in Fig. 2. The purpose of the circuit is to keep the BAT, PE and charger modules in the temperature regions that assure safety, suitable operation and reduce ageing caused by thermal stress. With this circuit, the heat generated in the electrical components due to the *Joule Effect* can be dissipated to the air or to the Air Conditioning (AC) circuit. Notice that:

- Only the driving situation is treated here, not the charging one. For this reason, the charger represents only a passive thermal mass in the circuit.
- The coolant is a water/glycol mixture and its possible paths are shown in the blue and black continuous lines in Fig. 2.
- The heat transfer with the air is done by means of a coolant/air heat exchanger, the cooler in Fig. 2.
- The heat transfer to the AC-circuit is done by a coolant/refrigerant heat-exchanger parallel to the evaporator called chiller in Fig. 2.

The heat transfer can be controlled through the coolant flow by six electrical actuators: two pumps, three solenoid valves and one fan, all in gray in Fig. 2. The control signals for these actuators are from the right top clockwise:

- $Valve_{COOLER}$ : Enables/disables the coolant flow through the cooler. With the value “0” the valve allows the cooler path, while “1” stands for the bypass.
- $PWM_{FAN}$ : The fan increases the air mass flow rate in front of the cooler and thus the heat exchange.

It is controlled by a pulse width modulated (PWM) signal.

- $PWM_{PE}$ : The electrical pump before the PE is also governed by a PWM signal.
- $Valve_{CHILLER}$ : Enables/disables the coolant flow through the chiller. The value “1” is for chiller active, “0” stands for chiller inactive.
- $Valve_{CIRCUIT}$ : Enables switching between big/small circuit configurations. If  $Valve_{CIRCUIT}$  is set to “1”, the big circuit configuration is active and the coolant flows through the charger, the cooler, the chiller, the BAT and the PE, consecutively. On the contrary, if  $Valve_{CIRCUIT}$  is set to “0”, the coolant flows through two separate circuits: the BAT-chiller circuit and the charger-cooler-PE circuit. Consequently, in this mode, the heat transfer between the BAT-chiller and the PE-charger-cooler is disabled. Notice that to propel the coolant in two different separated circuits, two electric pumps are required.
- $PWM_{BAT}$ : The electrical pump in front of the chiller is also governed by a PWM signal.

As said in the introduction, the high number of electrical actuators offers an accurate TM but also supposes a challenge in efficiency: to spend as less electrical energy as possible. With the control methodology described in Section III, the aim is to formulate and solve this problem.

### III. MODELING AND OPTIMAL CONTROL PROBLEM FORMULATION

The development of a system model is a crucial step for the NMPC strategy since it provides the predictive ability. The model of the cooling circuit in Fig. 2 is a system of ordinary differential equations (ODE) of the following general form:

$$\dot{x}(t) = f(x(t), u(t), p) \quad (1)$$

where  $x \in \mathbb{R}^{n_x}$  represents the states of the plant,  $u \in \mathbb{R}^{n_u}$  stands for the control inputs and  $p \in \mathbb{R}^{n_p}$  for the time-invariant parameters. It is important to highlight that all the states  $x$  are available from sensors equipped in the real vehicle.

Given the complexity and length of the mathematical model of the considered system, the reader can find its main lines in [8]. The interaction of the variables and constitutive elements of the resultant model are shown in Fig. 3. The model has been written in the software Dymola [9], which is based on the object-oriented language Modelica [10] and is a combination of physical equations and measurements stored in look-

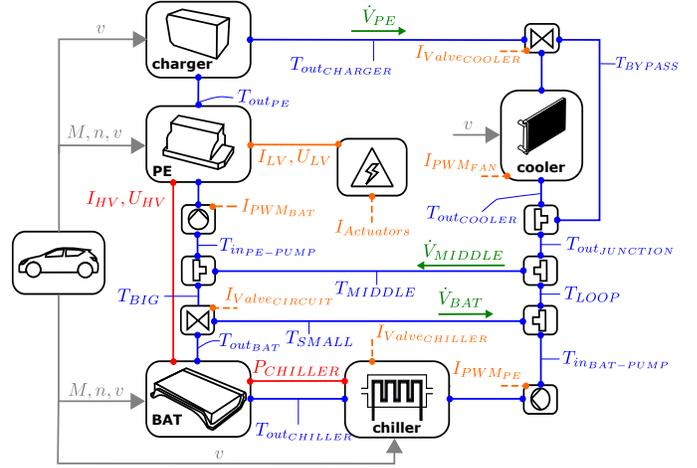


Fig. 3: Main variables and elements of the cooling circuit model in Modelica.

up tables that describe the cooling circuit behavior in multiple domains.

The physical equations of the model come mainly from energy balances. In the thermal domain, for instance, at each electric component the first thermodynamic law, (2), is applied to describe how the heat flow induced by the *Joule effect*  $\dot{Q}_{induced}$  is dissipated in the coolant  $\dot{Q}_{coolant}$ , the ambient air  $\dot{Q}_{ambient}$  and the component itself  $\dot{Q}_{thm}$ , that is,

$$\begin{aligned} \frac{dU(t)}{dt} &= \dot{Q}_{thm}(t) \\ &= \dot{Q}_{induced}(t) - \dot{Q}_{ambient}(t) - \dot{Q}_{coolant}(t). \end{aligned} \quad (2)$$

The model consists of around 500 equations and 1300 variables that arise from the equations explicitly described inside the different submodels and the automatic generated connection equations. With the help of the model-export methodology described in [11], it is quite straightforward and error-free to pass the high number of equations to the MUSCOD-II.

To get an overview of the system states contained in the dynamic model, (3) corresponds with a condensed form of the model, where the relation between the variables used here and the control inputs can be found in [8].

Furthermore, to measure the performance of the system, a so called objective or cost function was developed. This cost function is an indirect measurement of the system performance. To this end, the performance indices of Fig. 4 are used to evaluate the TM in terms of accuracy and efficiency.

The cost term  $c_T$  (on the left of Fig. 4) describes, with the following polynomial, the effect of the working temperature on the battery, so that the further from the

$$\dot{\mathbf{x}}(\mathbf{t}) = \mathbf{f}(\mathbf{x}(\mathbf{t}), \mathbf{u}(\mathbf{t}), \mathbf{p}) \quad (3)$$

$$\begin{bmatrix} \frac{dT_{inPE-PUMP}}{dt} \\ \frac{dT_{inBAT-PUMP}}{dt} \\ \frac{dT_{outJUNCTION}}{dt} \\ \frac{dT_{outCHILLER}}{dt} \\ \frac{dT_{outCHARGER}}{dt} \\ \frac{dT_{outPE}}{dt} \\ \frac{dE_{BAT}}{dt} \\ \frac{dT_{outBAT}}{dt} \\ \frac{dT_{outCOOLER}}{dt} \\ \frac{dv}{dt} \\ \frac{dM}{dt} \\ \frac{dn}{dt} \\ \frac{dT_{ambient}}{dt} \end{bmatrix} = \begin{bmatrix} \frac{\dot{m}_{MIDDLE} T_{MIDDLE} + \dot{m}_{BIG} T_{BIG} + \dot{m}_{inPE-PUMP} T_{inPE-PUMP}}{m_{VALVE}} \\ \frac{\dot{m}_{LOOP} T_{LOOP} + \dot{m}_{SMALL} T_{SMALL} + \dot{m}_{inBAT-PUMP} T_{inBAT-PUMP}}{m_{VALVE}} \\ \frac{\dot{m}_{outCOOLER} T_{outCOOLER} + \dot{m}_{BYPASS} T_{BYPASS} + \dot{m}_{outJUNCTION} T_{outJUNCTION}}{m_{VALVE}} \\ \frac{Q_{thm}}{m_{CHILLER} c_{PCHILLER}} \\ \frac{Q_{thm}}{m_{CHARGER} c_{PCHARGER}} \\ \frac{Q_{thm}}{m_{PE} c_{PPE}} \\ P_{HV} + P_{LOSSBAT} \\ \frac{Q_{thm}}{m_{BAT} c_{PBAT}} \\ \frac{Q_{thm}}{m_{COOLER} c_{PCOOLER}} \\ 0 \\ 0 \\ 0 \\ 0 \end{bmatrix}$$

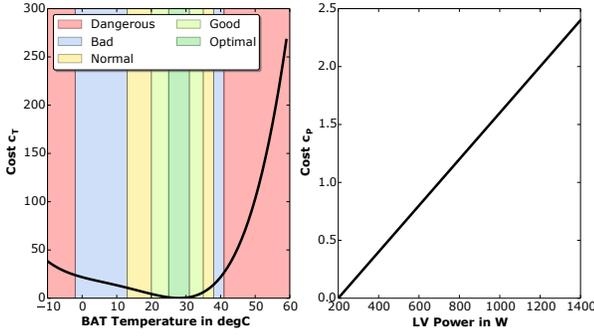


Fig. 4: Cost terms included in the objective function to evaluate accuracy and efficiency of the TM.

optimal range, the more promoted the aging mechanisms, i.e.,

$$c_T(T) = a_4 T^4 - a_3 T^3 + a_2 T^2 - a_1 T + a_0, \quad (4)$$

where  $a_0, a_1 \dots a_4$  are the corresponding parameters resultant from the curve fitting. The penalty term  $c_P$  (on the right of Fig. 4) is the following linear function depending on the electrical power  $P$  of the actuators:

$$c_P(P) = \frac{P - b_0}{b_1}, \quad (5)$$

where again  $b_0, b_1$  are calibration parameters. Besides,  $c_P$  indicates that the more electrical power is used for the TM, the less attractive it is. Table I shows the electrical actuators used categorizing them according to the amount of electric power they require. The total cost associated to the TM is given by  $c$ , which is the sum of

TABLE I: Actuators electrical power

Actuator	Control Signal	Electrical power
Cooler valve	$Valve_{COOLER} \in \{0, 1\}$	low
Fan	$PWM_{FAN} \in [10, 90]$	high
BAT pump	$PWM_{BAT} \in [0, 100]$	medium
Chiller valve	$Valve_{CHILLER} \in \{0, 1\}$	low
Compressor	$Valve_{CHILLER} \in \{0, 1\}$	high
Circuit valve	$Valve_{CIRCUIT} \in \{0, 1\}$	low
PE pump	$PWM_{PE} \in [0, 100]$	medium

the two penalty terms in Fig. 4, i.e.,

$$c = c_T + c_P. \quad (6)$$

Besides the model and objective function, the physical constraints definition is an important step in the control problem formulation. Hence, the saturation limits of the control signals, middle column in Table I, were defined as minimal and maximal constraints.

Nevertheless, for the PWM input signals of the pumps, more restrictive minimal constraints were used. They are

$$\begin{bmatrix} 16 \\ 30 \end{bmatrix} \leq \begin{bmatrix} PWM_{BAT} \\ PWM_{PE} \end{bmatrix}. \quad (7)$$

With these restrictive constraints it is assured that a minimal coolant amount flows through the components to protect them from a sudden change in temperature.

Similarly to the control signals, the constraints for the system states are defined as follows:

$$\begin{array}{c}
\mathbf{x}_{min} \\
-10^\circ\text{C} \\
-10^\circ\text{C} \\
-10^\circ\text{C} \\
-10^\circ\text{C} \\
-10^\circ\text{C} \\
-10^\circ\text{C} \\
1\text{ kWh} \\
-10^\circ\text{C} \\
-10^\circ\text{C} \\
-10\text{ km/h} \\
-500\text{ Nm} \\
-10^4\text{ rpms} \\
-10^\circ\text{C}
\end{array}
\leq
\begin{array}{c}
\mathbf{x} \\
T_{inPE-PUMP} \\
T_{inBAT-PUMP} \\
T_{outJUNCTION} \\
T_{outCHILLER} \\
T_{outCHARGER} \\
T_{outPE} \\
E_{BAT} \\
T_{outBAT} \\
T_{outCOOLER} \\
v \\
M \\
n \\
T_{ambient}
\end{array}
\leq
\begin{array}{c}
\mathbf{x}_{max} \\
65^\circ\text{C} \\
65^\circ\text{C} \\
65^\circ\text{C} \\
65^\circ\text{C} \\
65^\circ\text{C} \\
65^\circ\text{C} \\
8\text{ kWh} \\
65^\circ\text{C} \\
65^\circ\text{C} \\
200\text{ km/h} \\
500\text{ Nm} \\
10^4\text{ rpms} \\
65^\circ\text{C}
\end{array}, \quad (8)$$

178 where it must be highlighted that the maximal working  
179 temperature for the coolant in this circuit is  $65^\circ\text{C}$ .

With all these requirements, the open-loop finite-horizon optimal control problem (OCP) associated to the cooling circuit can be formulated as follows:

$$\min_{x^*(\cdot), u^*(\cdot)} \int_{t_0}^{t_0+H_p} (c_T + c_P) dt \quad (9a)$$

subject to

$$\dot{x}(t) = f(x(t), u(t), p) \quad \forall t \in \tau \quad (9b)$$

$$x_{min} \leq x \leq x_{max} \quad \forall t \in \tau \quad (9c)$$

$$u_{min} \leq u \leq u_{max} \quad \forall t \in \tau \quad (9d)$$

$$0 = x(t_0) - x_0. \quad (9e)$$

180 Given an initial value of the states,  $x_0$ , at time  $t_0$ , the  
181 goal of the strategy is to find the optimal sequence of  
182 control inputs and states,  $u^*(\cdot), x^*(\cdot)$ , that minimizes the  
183 objective function in (9a), and satisfy the constraints in  
184 (9b-9e), for a given prediction horizon of length  $H_p$ .

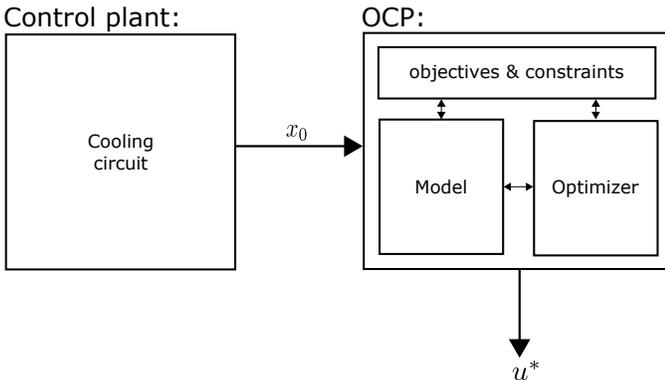


Fig. 5: Optimal control problem outline

#### IV. NUMERICAL SOLUTION OF THE NMPC PROBLEM 185

To attend model-plant mismatches and overcome possible disturbances, the open-loop scheme in Fig. 5 must be closed resulting in the NMPC scheme in Fig. 6. The main idea behind NMPC is to formulate and solve repetitively a new OCP at each time instant according to the receding horizon strategy. At a certain instant  $k$ , the measurement of the plant  $x$  is used to initialize the ODE with  $x(t_0) = x$  used in the constraint (9e) and the OCP is solved to find the optimal control sequence  $u^*$  for the given prediction horizon. From the solution sequence  $u^*$ , only the first element is applied to the system and the whole procedure is repeated for the next time instant  $k + 1$  with new sensors measurements coming as the closed-loop system feedback, thus receding the prediction horizon.

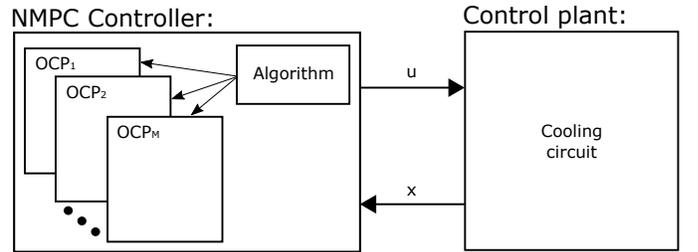


Fig. 6: Control scheme of NMPC

There exist several numerical methods for solving an OCP, as reported in [12]. The optimization tool used in this research, MUSCOD-II, relies on efficient and robust DMS algorithm [13] that reformulates the OCP as a non-linear programming (NLP) problem that is then solved by an iterative solution procedure, a specially tailored Sequential Quadratic Programming (SQP) algorithm [6]. Notice that the discretization of the continuous optimal control problem is done inside MUSCOD-II. At each time instant, the MSP discretizes the OCP horizon with the following N-points grid:

$$0 = \tau_0 < \tau_1 < \dots < \tau_N = t_f. \quad (10)$$

Fig. 7, an example of an optimization horizon of length  $t_f$  divided in  $N = 4$  intervals with five MS points is shown, where it can be seen how one of the thirteen differential states,  $x[k]$ , and one of the six controls,  $u[j]$  are discretized according to the MS scheme.

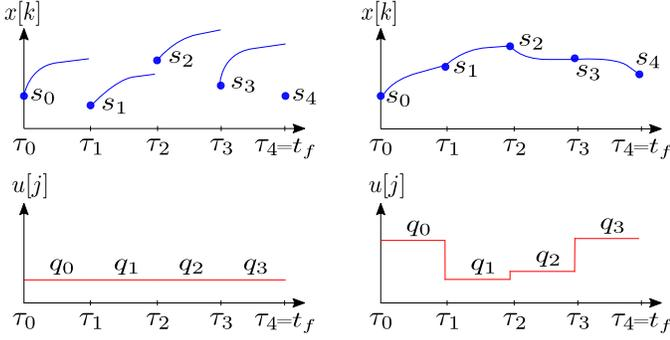


Fig. 7: Multiple shooting method with a grid of 5 shooting points before (left plots) and after (right plots) convergence is achieved.

206 The left plots in Fig. 7 show the start of the optimiza-  
 207 tion and the right ones belong to the situation once the  
 208 process has converged. As it can be seen, inside each  
 209 interval, the controls are parametrized as follows:

$$u(t) := q_i, \quad t \in [\tau_i, \tau_{i+1}) \quad (11a)$$

where  $q_i \in \mathbb{R}$ . Additionally, at each grid point new initial values  $s_i$  are added. Combining an integrated ODE solver for solving the resulting initial value problems (IVP) and the SQP algorithm, the optimizer searches the controls  $q_0, q_1 \dots q_{N-1}$  and shooting points  $s_0, s_1, s_2 \dots s_{N-1}$  that minimize the objective function and fulfill the constraints. In other words, the optimizer solves the following NLP problem:

$$\min_{\xi} \sum_{i=0}^N l_i(\tau_i, s_i, q_i, p) \quad (12a)$$

subject to

$$s_{i+1} = x_i(\tau_{i+1}; \tau_i, s_i, q_i, p) \quad 0 \leq i \leq N-1, \quad (12b)$$

$$0 \leq c(\tau_i, s_i, q_i, p), \quad 0 \leq i \leq N \quad (12c)$$

$$0 = s_0 - x_0 \quad (12d)$$

210 where  $\xi = (q_0, q_1 \dots q_{N-1}, s_0, s_1, s_2 \dots s_{N-1})$  is a vector  
 211 with all the unknowns and  $x_i(\tau_{i+1}; \tau_i, s_i, q_i, p)$  denotes  
 212 the solution of the IVP on the shooting interval  $i$ ,  
 213 evaluated in  $\tau_{i+1}$ , and depending on the initial time  $\tau_i$ ,  
 214 initial state  $s_i$ , controls  $q_i$  and model parameters  $p$ . The  
 215 constraint (12b) forces that the trajectory at the end of  
 216 one interval matches the initial values of the trajectory  
 217 in the next interval and thus the whole continuity can  
 218 be assured after convergence is achieved, as it can be  
 219 seen on the right plots in Fig. 7. Moreover, the constraint  
 220 (12c) collects the discretized path constraints in (9b)-(9d)  
 221 while (12d) is the discretized version of (9e).

222 Finally, it must be added that MUSCOD-II relies  
 223 on the so called Real-Time Iteration (RTI) scheme for

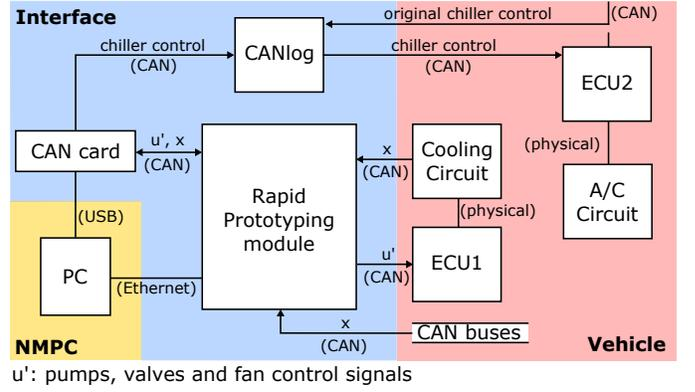


Fig. 8: Hardware implementation for the cooling circuit control manipulation.

achieving robust online performance. The main idea  
 of this algorithm is to exploit the similarity between  
 subsequent OCP for performing the SQP steps in a  
 different order as accustomed, prioritizing this way a  
 fast response time to disturbances. For more information  
 about the RTI scheme, the reader is referred to [14].  
 It must be added that the state of the plant, available  
 from several CAN buses, was sampled every 10 ms.  
 Nevertheless, the communication between the vehicle  
 and MUSCOD-II was asynchronous, being states and  
 controls exchanged as soon as MUSCOD-II performed  
 a new step with the RTI scheme. Using a prediction  
 horizon of 200 seconds and two shooting points, the  
 maximal measured response time of MUSCOD-II was  
 2.5 s, which is quite acceptable for the studied thermal  
 system inertia.

## V. HARDWARE IMPLEMENTATION

The PHEV used in this research is a prototype of  
 a Golf GTE equipped with extra sensors placed in the  
 cooling circuit to read all relevant information. In total,  
 17 thermocouples of type K with accuracy of  $\pm 1^\circ\text{C}$   
 were used to measure 15 coolant temperatures, the air  
 temperature in front of the cooler and the air temperature  
 on the roof of the vehicle. In addition, three turbine flow  
 meters with a linearity of 0.1% were used to measure the  
 coolant volume flow rate.

With the aim of being able to compare the standard  
 control with the NMPC in successive driving tests, the  
 design in Fig. 8 was implemented. With this implemen-  
 tation, it can be switch between two operation modes as  
 explained next.

### A. NMPC Mode

MUSCOD-II runs in the Laptop held by the co-pilot,  
 being connected to a rapid prototyping (RP) module

258 through an Ethernet connection. The control signals are  
 259 sent by means of the Universal Serial Bus (USB) con-  
 260 nected Controller Area Network (CAN) card to the RP  
 261 module. The electronic control unit (ECU1) is equipped  
 262 with an emulator test probe (ETK) that allows that the  
 263 control signals arriving to the ECU1 via the RP ETK  
 264 connection, are taken instead of the original code in the  
 265 ECU1 software. This way the original physical electric  
 266 connections to the actuators in the cooling circuit can  
 267 be kept. Furthermore, the states of the controlled plant,  
 268 output signals of the temperature sensors installed in the  
 269 cooling circuit and other signals running in the CAN  
 270 buses of the vehicle are sent to MUSCOD-II through  
 271 the RP module.

272 Since the chiller valve is physically stimulated from  
 273 another ECU (ECU2) that is not equipped with ETK, a  
 274 CAN logger is needed (top right corner of Fig. 8). The  
 275 CAN logger performs a gateway that splits the CAN bus  
 276 containing the original command for this valve. This way  
 277 the  $Valve_{CHILLER}$  calculated in MUSCOD-II can be  
 278 used instead of the original vehicle demand.

### 279 B. Standard Mode

280 The RP deactivates the bypass of ECU1 and the CAN  
 281 logger sends the signal arriving from the original CAN  
 282 bus to the ECU2. In this mode, the original control  
 283 signals of the vehicles for the cooling circuit and AC  
 284 circuit are taken. These control signals are set to constant  
 285 values output by a finite-state machine with four possible  
 286 states: heating, temperature maintaining, mild cooling  
 287 and maximal cooling. The conditions for changing from  
 288 one state to another depend on the current BAT temper-  
 289 ature and some sensors describing the availability of the  
 290 heat exchangers to dissipate the heat.

## 291 VI. DRIVING SCENARIOS

292 A requirement for testing the TM of electric compo-  
 293 nents is to choose a driving cycle in which significant  
 294 thermal load is generated. This can be achieved with  
 295 a heavy load cycle driven in the pure electric mode  
 296 since the heat generated in the components is caused  
 297 by the *Joule Effect*. To design a driving cycle with a  
 298 heavy mechanical demand, three different scenarios were  
 299 chosen to be performed on an open-accessible street with  
 300 low traffic density:

- 301 • **Long cycle mild:** A long trip of 39 km in a road  
 302 with considerable slope in mild climate conditions.
- 303 • **Long cycle hot:** The same cycle in hot climate  
 304 conditions.
- 305 • **Constant cycle:** A trip at 100 km/h constant speed  
 306 in a 21 km road also with considerable slope.  
 307

A key aspect of these cycles is the effort put in the  
 design to make them as repeatable as possible. Quite  
 helpful for this task is the adaptive cruise control (ACC)  
 that is available in the car. Other cars are obstacles  
 in the road that prevent the vehicle from following  
 the repeatable cycle forcing the driver to accelerate or  
 break abruptly and therefore they can be considered as  
 external disturbances. Due to the usage of the ACC,  
 these disturbances are held to a minimum since the ACC  
 accelerates and decelerates smoothly, in contrast to the  
 driver natural reaction, thus generates minimal extra load  
 to the battery.

Additionally to achieve always a similar electrical  
 power demand to the BAT, all the tests were driven  
 with the car being under the same conditions. Auxiliary  
 consumers like heating, air conditioning and ventilation  
 (HVAC) were turned off, as well as lights, radio and  
 other electrical gadgets. Windows were opened to the  
 same level and the weight of the car was held the same.

To assure similar initial conditions, it is specially cru-  
 cial to monitor the BAT temperature before driving, since  
 as it takes direct influence on the objective function,  
 small discrepancies in it will lead to non comparable  
 conditions for the two cycles. Thus, the car is always  
 fully charged the day before in order to assure that all  
 temperatures in the car were close to the ambient tem-  
 perature and not disturbed by any heat source and that  
 the BAT draws always from with the same energy level.  
 This way, once enough similar conditions are observed,  
 ambient, battery temperatures and traffic congestion, a  
 comparable driving cycle can be assured and the test  
 can start. As it will be seen in the Section VII, this test  
 procedure enabled enough repeatable driving cycles to  
 compare the results of performing a different control in  
 the cooling circuit.

## VII. RESULTS

Experimental results from the three different cycles  
 will be discussed in the following subsections. They are  
 also summarized in Table II, where the consumption,  $E$ ,  
 cost terms,  $c_T$  and  $c_P$  and total cost,  $c$ , are compared for  
 the two operation modes, NMPC and standard, described  
 in Section V. Notice that in Table II a negative value  
 represents a decrease of the cost comparing NMPC to  
 the standard strategy.

### A. Long cycle mild

As it can be seen in the top plot in Fig. 9, where the  
 left y-axis shows the vehicle speed and the right one the  
 altitude of the road, the long cycle consists of a highway  
 road section, in blue, followed by a mountain that is

TABLE II: NMPC vs standard results in TM for three different driving cycles.

Cycle	$\Delta E^*$ in kWh	$\frac{\Delta E^{**}}{E_0}$ in %	$\frac{\Delta c_T}{c_{T_0}}$ in %	$\frac{\Delta c_P}{c_{P_0}}$ in %	$\frac{\Delta c}{c_0}$ in %
Long cycle mild	-0.015	<b>-6.25</b>	-8.1	-20.71	<b>-9.95</b>
Long cycle hot	-0.027	<b>-8.14</b>	-54.26	-17.12	<b>-50.04</b>
Constant cycle	0.003	<b>3.49</b>	-8.2	5.09	<b>-7.78</b>

\*  $\Delta x$  stands for the measured difference in the value “x”:  $x_{NMPC} - x_{Standard}$ .

\*\*  $x_0$  stands for the measured value “x” in the Standard cycle:  $x_{Standard}$ .

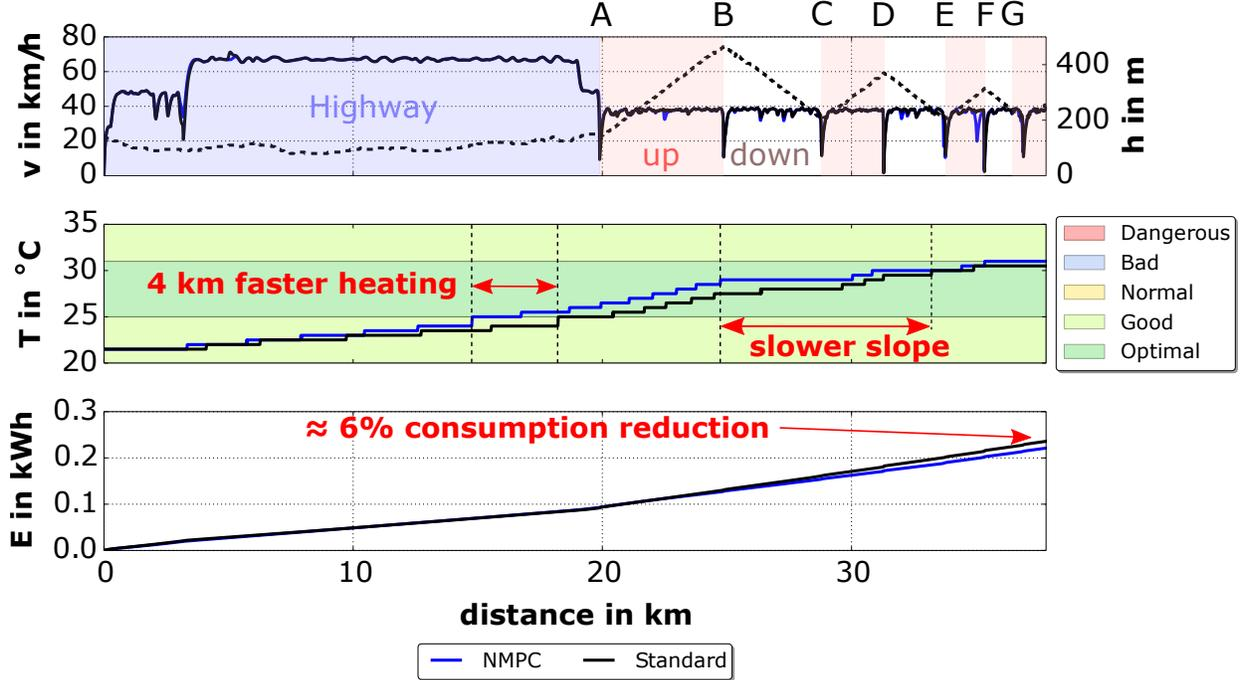


Fig. 9: NMPC vs standard TM results in terms of temperature accuracy and electrical consumption of the actu in the long cycle mild.

357 ascended to the top, in red, discharging the battery and  
 358 then descended to the bottom, in white, charging the  
 359 battery again.

360 The aim of this driving cycle is to keep the BAT  
 361 working and thus generating heat as much time as  
 362 possible under heavy conditions. To achieve this, in the  
 363 slope road section several strategic turning points were  
 364 predefined. This way, the vehicle faces the slope for  
 365 the first time at A and drives till the highest point B  
 366 is reached, where the vehicle turns over and starts the  
 367 descent to the initial kilometric point A, now named C  
 368 in Fig. 9. Again, the vehicle turns over and drives to  
 369 the next turning point, D, lower than B and so on till,  
 370 after the last turn over in G, the BAT is fully discharged  
 371 and the pure electric mode is no longer available. The  
 372 small variations in the speed profile during NMPC (blue  
 373 solid line) and standard control (black solid line) allow to  
 374 assume that the results discussed draw from comparable

conditions.

375

In the middle and bottom plots in Fig. 9, the TM  
 resulting from the NMPC and standard strategies in  
 a mild thermal scenario, ambient temperatures around  
 14°C and initial BAT temperature 22°C, can be com-  
 pared. Concerning the goal of keeping the battery within  
 optimal temperatures, it can be seen in the middle plot  
 that NMPC reaches the optimal range about 4 km faster  
 than the standard control strategy. Once inside this range,  
 the slope decreases to maintain the BAT at this level.  
 Moreover, the second goal, the electric consumption  
 shown in the plot on the bottom, is reduced by 6%. The  
 NMPC success in multiple objective achievements can  
 be seen in detail in Fig. 10. Focusing on the temperature  
 and consumption related costs of NMPC, blue line in  
 the top and middle plot in Fig. 10, respectively, three  
 differentiated strategic phases for the control can be  
 derived: 1) Battery heating phase (blue area in Fig. 10) in

376  
377  
378  
379  
380  
381  
382  
383  
384  
385  
386  
387  
388  
389  
390  
391  
392

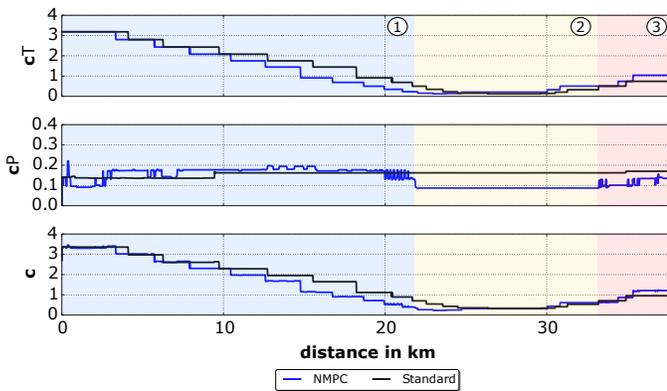


Fig. 10: NMPC vs standard objective function costs.

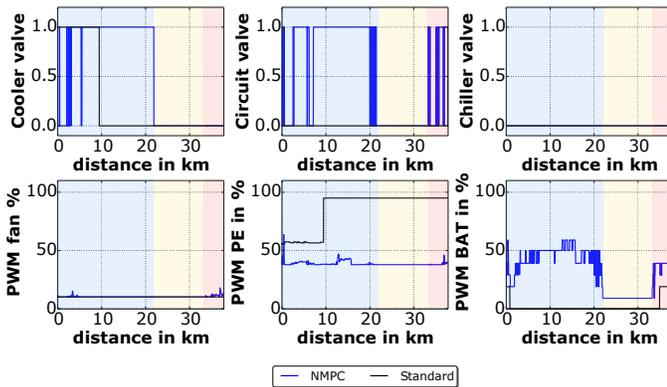


Fig. 11: NMPC vs standard control strategies in the long cycle mild.

393 which the main goal is to bring the battery temperature to  
 394 the optimum as it is shown in the top plot with the faster  
 395 decrease of the temperature cost in NMPC inside the  
 396 blue area. The prize to pay is a slightly higher electrical  
 397 consumption as represented in the middle plot, 2) Energy  
 398 saving phase (yellow area in Fig. 10) where the priority  
 399 is to minimize the actuators electrical consumption as  
 400 it can be seen clearly in the yellow area of the middle  
 401 plot and 3) Battery cooling phase (red area in Fig. 10)  
 402 in which the temperature costs, this time associated to  
 403 higher temperatures than the optimal, are again high  
 404 enough to invest resources. Inside the different described  
 405 phases, the control inputs from the NMPC strategy show  
 406 a tendency as it can be seen in Fig. 11.

407 For heating the BAT, the cooler valve is bypassed and  
 408 the circuit valve enables the big circuit mode that couples  
 409 the BAT and the PE. As Fig. 12 shows, this is a clever  
 410 way to heat the BAT since compared to it, the PE has a  
 411 higher temperature and the air flowing through the cooler  
 412 a lower one.

413 Once the optimal temperature is achieved, as shown  
 414 in Fig. 12, the cooler is activated as well as the two  
 415 circuit mode. The BAT is decoupled from the PE at

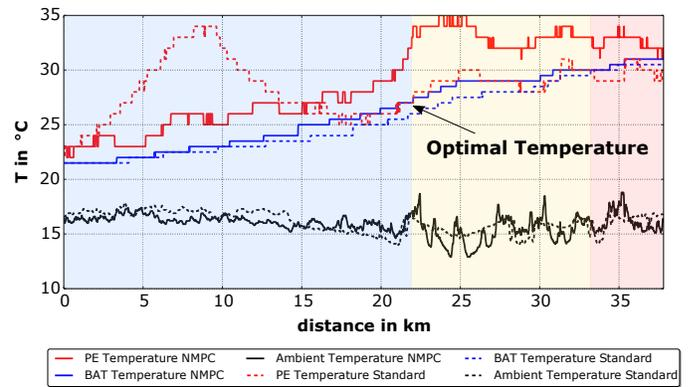


Fig. 12: NMPC vs standard components and ambient temperatures in the long cycle mild.

this moment, because the PE is warmer and the BAT 416  
 is already at its optimal temperature. The reason for the 417  
 cooler activation is to dissipate to the air the heat that 418  
 is being generated in the PE module due to the road 419  
 slope. This way, the constraint of not exceeding 65°C in 420  
 this module is achieved. It must also be said that, in this 421  
 phase (yellow area), the battery pump is brought down to 422  
 its minimum in order to save energy. As soon as the BAT 423  
 temperature starts deviating from the optimal one, about 424  
 3°C, the circuit valve enables and disables the coupling 425  
 to the PE circuit intermittently. 426

### B. Long cycle hot 427

428 The same cycle was driven under hotter conditions 429  
 having been the vehicle parked outdoors, exposed to direct 430  
 sunlight: average ambient temperature around 20°C 431  
 and initial BAT temperature 31-31.5°C. Again, despite 432  
 some punctual speed discrepancies due to different traffic 433  
 situations, the cycles in Fig. 13 are enough similar to be 434  
 compared.

435 As it can be seen in Table II, in this cycle there 436  
 is even more potential than in the mild climate case. 437  
 The consumption is reduced this time by 8% while the 438  
 temperature trajectory is more accurate, temperatures 439  
 closer to the optimal range, than with the standard 440  
 control. The combination of these two goals leads to a 441  
 numerical improvement of 50% in the objective function. 442  
 In general, it can be said that the more cooling requiring 443  
 the situation is, the more potential NMPC has. This 444  
 is due to the fact that the studied cooling circuit has 445  
 several heat sinks for actively cooling the components 446  
 but no heat sources for heating the battery. That means 447  
 that under cold conditions, the only possibility is to take 448  
 advantage from the different inertias of the components 449  
 in the system while under hot conditions, the many 450  
 cooling alternatives lead to completely different results.

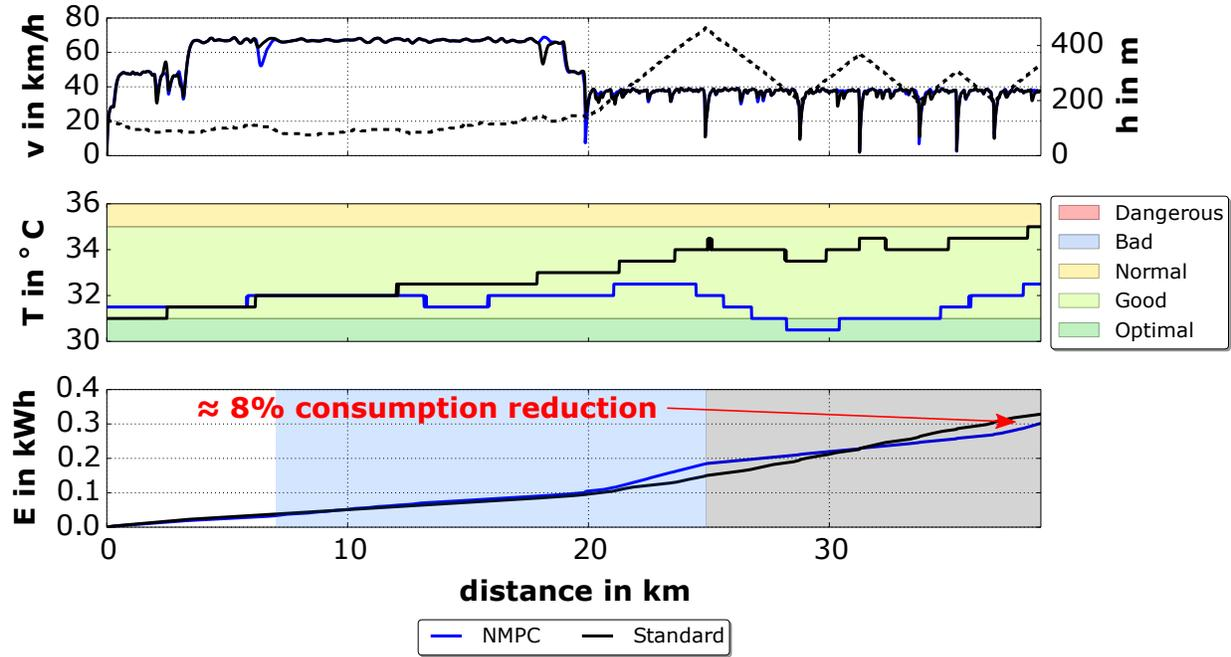


Fig. 13: NMPC vs standard TM results in terms of temperature accuracy and electrical consumption of the actuators in the long cycle hot.

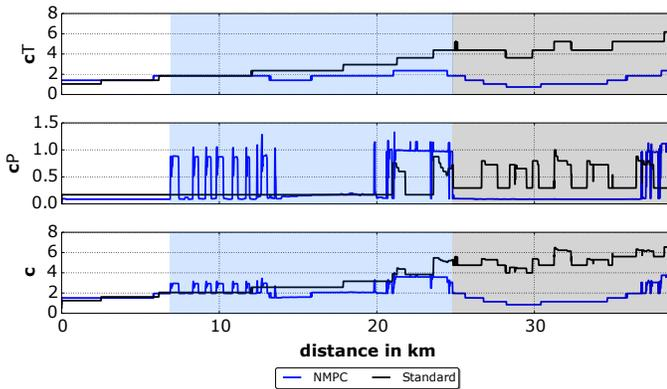


Fig. 14: NMPC vs standard objective function costs in the long cycle hot.

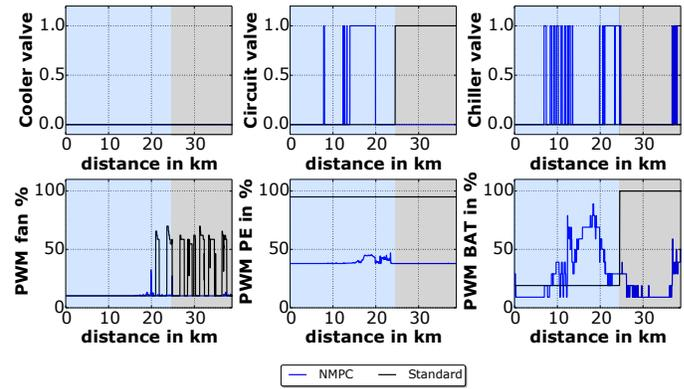


Fig. 15: NMPC vs standard control strategies in the long cycle hot.

451 The blue and black areas in Fig. 14 show the intervals in which most cooling resources are invested for  
 452 NMPC and standard control strategies, respectively. As  
 453 it can be seen, NMPC starts investing in keeping the  
 454 BAT temperature closer to the optimal sooner than the  
 455 standard control strategy. Fig. 15 illustrates the different  
 456 use of the cooling resources of both strategies.

458 While NMPC invests in the chiller and moderately  
 459 in the pumps in an intermittent way to cool down the  
 460 BAT temperature, the standard control strategy shows  
 461 two clearly differentiated working points: previous to the  
 462 black region, it only uses the PE pump and the cooler  
 463 valve to cool down the PE and inside the black region, as

soon as the BAT temperature is too far from the optimum 464  
 it uses the pumps at full and the fan at medium power. 465

In Fig. 16 the BAT, PE and ambient temperatures 466  
 for both cycles are compared. Although the ambient 467  
 temperature at the end of the cycle, last 25 km, is lower 468  
 in the standard cycle, the NMPC strategy achieves a 469  
 more accurate regulation of the BAT temperature. Notice 470  
 also that both PE curves are far away from the critical 471  
 temperature of  $65^{\circ}\text{C}$  for the component, imposed in the 472  
 NMPC case by means of a constraint. 473

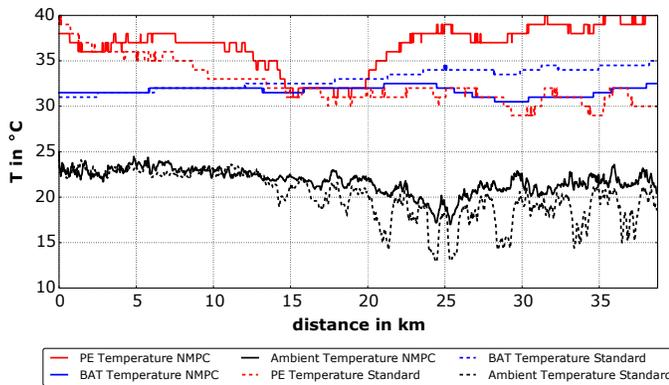


Fig. 16: NMPC vs standard components and ambient temperatures in the long cycle hot.

### 474 C. Constant cycle

475 The constant driving cycle consists of the entrance to  
 476 the highway, first 4 km in Fig. 17, and then the drive on  
 477 the highway at constant speed of 100 km/h. The highway  
 478 road has a considerable slope that, together with the high  
 479 speed, leads to the full discharge of the BAT in the 17  
 480 minutes duration of the whole cycle. Again, the TM with  
 481 the NMPC presents a decrease in the global cost function  
 482  $c$  of Table II compared to the standard control. Although,  
 483 the electrical consumption of the actuators is increased  
 484 by 3.5%, as it can be seen in Fig. 17, the faster heating  
 485 of the BAT to the optimal temperature compensates this  
 486 loss.

487 One of the main reasons for these results being less  
 488 attractive than in the other driving cycles is that this one  
 489 starts at colder temperatures, the initial BAT temperature  
 490 is 14°C, and thus the potential of the system is reduced.  
 491 The cooling circuit has several options for cooling the  
 492 BAT, the cooler and chiller, but for generating heat it can  
 493 only wait to use the heat generated in the PE, which has  
 494 a lower thermal mass.

495 As shown in Fig. 18 and in contrast to the costs within  
 496 the long cycle in Fig. 10, here NMPC follows nearly all  
 497 the cycle long the same strategy, to reduce the penalty  
 498 term  $c_T$ . Only at the end, after 20 km, it starts to play  
 499 with the chiller valve as shows the red arrow in Fig. 18.

500 It must be added that the fact that this cycle is driven  
 501 at constant speed, places the standard strategy in an  
 502 advantageous situation, since finite-state machines are  
 503 usually defined with several static points at which control  
 504 experience is available. Therefore, the less transient and  
 505 the more common the driving conditions are, the more  
 506 accurate is this method. In this case, the standard finite-  
 507 state machine shows two fixed operation points as it can  
 508 be seen with the black solid lines in Fig. 19.

509 Moreover, it must be added that the last 5 km of this

cycle are not as comparable as desired, since as it is  
 shown in Fig. 20 the ambient temperature in the NMPC  
 case is around 3°C above the standard control case.  
 This fact could be an extra disadvantage for the NMPC  
 since this happened when the BAT was already close to  
 the optimal temperature and hence the cooling potential  
 through the air is less. Furthermore, the presence of some  
 traffic before ending the cycle, as it can be seen in Fig.  
 17, leads to a more abrupt deceleration and thus to a  
 higher heat generation in NMPC, being this a further  
 disadvantage at temperatures close to the optimal, as it  
 is the case.

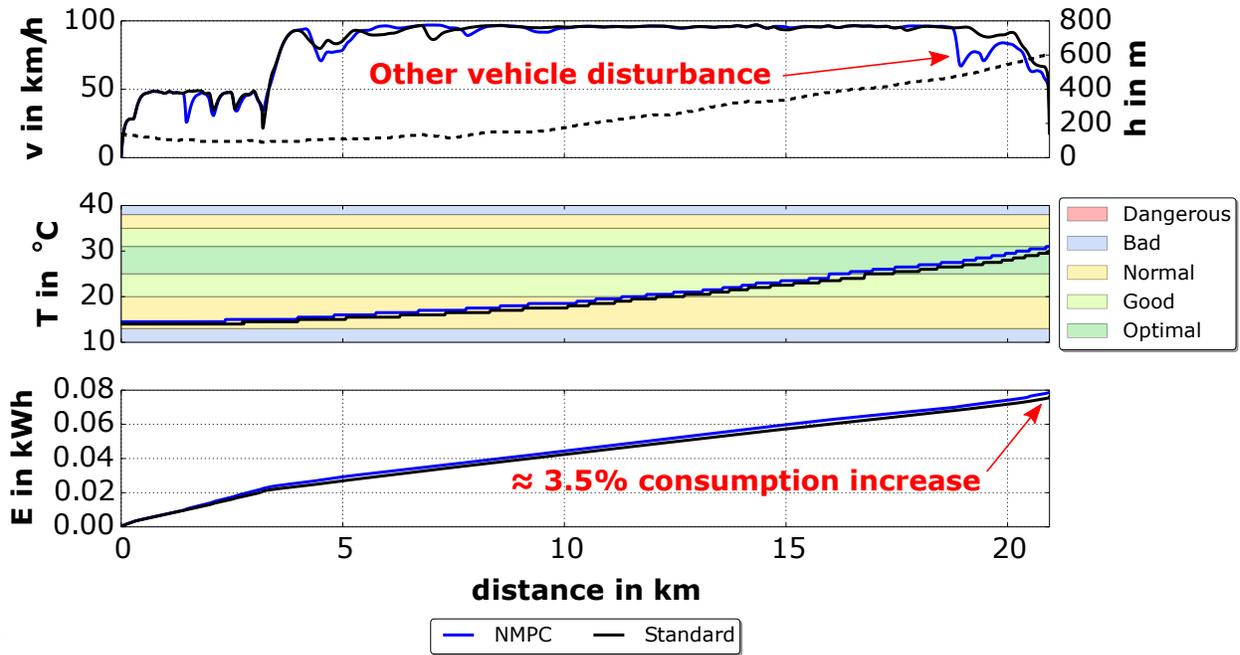
All in all, it can be said that even in an scenario  
 where the standard control strategy can show its major  
 performance, the NMPC still achieves a more accurate  
 TM. It must be also said that the fact that one goal, the  
 electrical consumption, becomes worse in favor of the  
 other goal, temperature regulation, is a mere strategic  
 matter. One of the advantages of the proposed NMPC  
 strategy is that terms in the objective function,  $c_T$  and  
 $c_P$ , can be changed or modified to achieve other results.  
 Compared to a PID tuning method, this calibration is  
 simpler since the parameters adjusted have a physical  
 meaning whose effect on the goals can be reproduced  
 and observed with a limited number of experiments or  
 simulations.

## VIII. CONCLUSIONS

In this paper, a real-time NMPC for the Li-ion battery  
 and power electronics cooling circuit in a PHEV proto-  
 type has been validated with three different repeatable  
 driving cycles performed on the road. In all studied  
 cases, NMPC has shown a significant decrease, from 7%  
 up to 50%, in the total costs associated to an accurate  
 and efficient TM when compared to a standard control  
 strategy based on a finite-state machine.

Analyzing the results according to the two objectives  
 separately, it can be said that the temperature cost was  
 reduced in the three studied cases while the electrical  
 consumption was reduced, between 6 and 8 %, only  
 in the long cycle tests. In the constant cycle it was  
 increased by 3.5%. Although the overall cost for this  
 cycle is already satisfactory, if additionally both goals  
 should be improved at the same time, it would be quite  
 straightforward to achieve adjusting the cost functions.  
 This is a further advantage in comparison with a PID  
 tuning process where the effect of the P, I and D gains  
 on the several goals are not so intuitively and directly  
 attributable to them.

This may seem paradoxical, but there are two reasons  
 for the constant cycle presenting the most moderate im-  
 provement of the three cycles. On the one hand, the cold



H

Fig. 17: NMPC vs standard TM results in terms of temperature accuracy and electrical consumption of the actuators in the constant cycle.

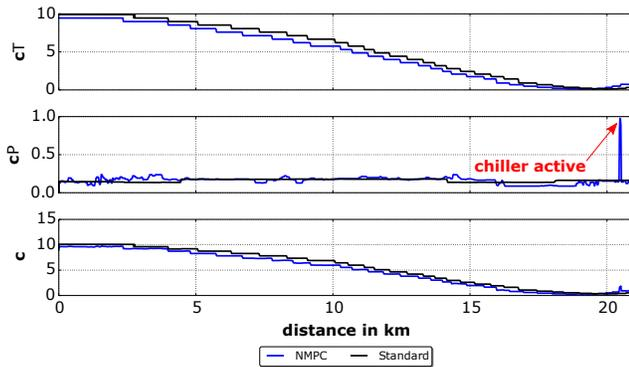


Fig. 18: NMPC vs standard objective function costs in the constant cycle.

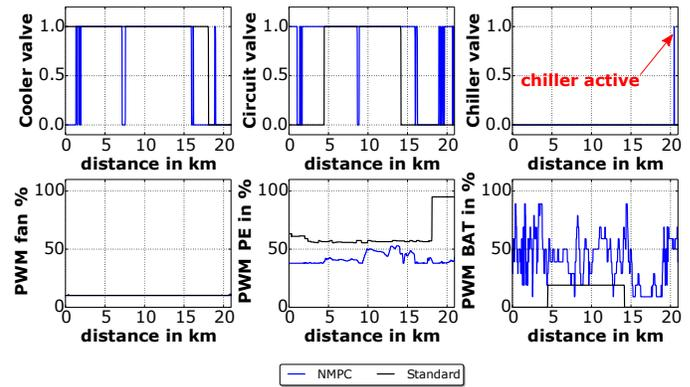


Fig. 19: NMPC vs standard control strategies in the constant cycle.

561 temperatures in this cycle reduce considerably the poten-  
 562 tial of the control strategy because the studied cooling  
 563 circuit cannot generate any other heat than the induced  
 564 by the Joule Effect. On the contrary, in a hot scenario  
 565 as in the long cycles studied, the heat dissipation can be  
 566 done to the ambient air or to the A/C circuit through the  
 567 several actuators, thus leading to many control options  
 568 for cooling the components. Therefore, it can be said  
 569 that under complex situations with many control options  
 570 NMPC methods show the highest potential. On the other  
 571 hand, the untapped potential of the standard strategy is  
 572 reduced in a quite steady cycle such as the constant cycle,  
 573 because finite-state machine are usually designed using  
 574 measured data at several stationary points. Nevertheless,

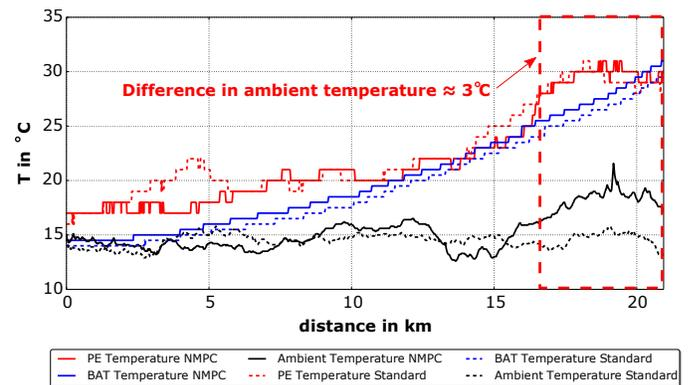


Fig. 20: NMPC vs standard components and ambient temperatures in the constant cycle.

575 it was shown that even in this situation, the NMPC is able  
 576 to grasp part of the untapped potential of the standard  
 577 strategy.

578 Finally, it must be concluded that the OCP formulated,  
 579 by means of a simple and accurate model, and the DMS  
 580 and RTI algorithm implemented in MUSCOD-II, have  
 581 led to an NMPC control strategy that has shown a stable  
 582 and real-time capable performance. Future works will be  
 583 focused on the improvement through the use of a driving  
 584 cycle prediction and the mixed-integer optimal control  
 585 problem (MIOCP) formulation and solution.

## 586 REFERENCES

- 587 [1] A. A. Pesaran, "Battery Thermal Management in EVs and  
 588 HEVs : Issues and Solutions," in *Advanced Automotive Battery  
 589 Conference*, Las Vegas, Nevada, 2001.
- 590 [2] R. Schmied, H. Waschl, R. Quirynen, and M. Diehl, "Nonlinear  
 591 MPC for Emission Efficient Cooperative Adaptive Cruise Con-  
 592 trol," in *5th IFAC Conference on Nonlinear Model Predictive  
 593 Control*, 2015.
- 594 [3] N. V. Duijkeren, T. Keviczky, and P. Nilsson, "Real-Time  
 595 NMPC for Semi-Automated Highway Driving of Long Heavy  
 596 Vehicle Combinations," in *5th IFAC Conference on Nonlinear  
 597 Model Predictive Control*, 2015.
- 598 [4] Z. Jiangyan, S. Tielong, S. Takanobu, and K. Masaaki, "Non-  
 599 linear MPC-Based Power Management Strategy for Plug-in  
 600 Parallel Hybrid Electrical Vehicles," in *Proceedings of the 33rd  
 601 Chinese Control Conference*, 2014.
- 602 [5] J. Zhao, S. Member, J. Wang, and S. Member, "Integrated  
 603 Model Predictive Control of Hybrid Electric Vehicles Coupled  
 604 with Aftertreatment Systems," *IEEE Transactions on Vehicular  
 605 Technology*, vol. 9545, no. Not published yet, but accepted for  
 606 a future issue., pp. 1–13, 2015.
- 607 [6] C. Hoffmann, L. Wirsching, M. Diehl, D. B. Leineweber,  
 608 A. A. S. Sch, H. G. Bock, and J. P. Schl, "MUSCOD-II user  
 609 manual," Heidelberg, 2010.
- 610 [7] H. Chen, S. Yu, X. Lu, F. Xu, T. Qu, and F. Wang, "Applying  
 611 Model Predictive Control in Automotive," in *Proceedings of the  
 612 10th World Congress on Intelligent Control and Automation*,  
 613 2012.
- 614 [8] J. L. Sanz, C. Ocampo-Martinez, J. Alvarez-Florez, M. M.  
 615 Eguilaz, R. Ruiz-Mansilla, J. Kalmus, M. Graber, and G. Lux,  
 616 "Nonlinear Model Predictive Control for Thermal Management  
 617 in Plug-in Hybrid Electric Vehicles," *IEEE Transactions on  
 618 Vehicular Technology*, vol. PP, no. 99, p. 1, 2016.
- 619 [9] D. AB, "Dymola Users Manual Version 5.3a," Lund, Sweden,  
 620 2004. [Online]. Available: <http://www.dynasim.com>
- 621 [10] M. Association, "Modelica - A Unified Object-Oriented  
 622 Language for Physical Systems Modeling Language  
 623 Specification," Modelica Association, Tech. Rep., 2010.  
 624 [Online]. Available: <http://www.modelica.org>
- 625 [11] M. Gräber, C. Kirches, D. Scharff, and W. Tegethoff, "Using  
 626 Functional Mock-up Units for Nonlinear Model Predictive  
 627 Control," in *Proceedings of the 9th International Modelica  
 628 Conference*, Munich, 2012.
- 629 [12] M. Diehl, H. J. Ferreau, and N. Haverbeke, "Efficient Numerical  
 630 Methods for Nonlinear MPC and Moving Horizon Estimation,"  
 631 in *Nonlinear Model Predictive Control*, L. et al Magni, Ed.  
 632 Springer, 2009, pp. 391–417.
- 633 [13] H. G. Bock and K. J. Plitt, "A multiple shooting algorithm for  
 634 direct solution of optimal control problems," in *Proceedings 9th  
 635 IFAC World Congress Budapest*, vol. XLII, 1984, pp. 243–247.

- [14] M. Diehl, H. G. Bock, J. P. Schlo, R. Findeisen, 636  
 Z. Nagy, and F. Allgo, "Real-time optimization and 637  
 nonlinear model predictive control of processes governed 638  
 by differential-algebraic equations," *Journal of Process 639  
 Control*, vol. 12, pp. 577–585, 2002. [Online]. Available: 640  
[www.elsevier.com/locate/jprocont](http://www.elsevier.com/locate/jprocont) 641